To be presented at the Conference on
Highly Excited States of Nuclei,
Julich, Germany, September 22 - 27, 1975

LBL-4311
c.1

EXPERIMENTAL STATUS OF HIGH-SPIN STATES

F. S. Stephens

September 1975

Prepared for the U. S. Energy Research and
Development Administration under Contract W-7405-ENG-48

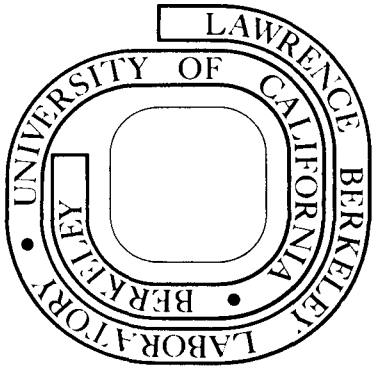

LBL-4311
c.1

DISCLAIMER

EXPERIMENTAL STATUS OF HIGH-SPIN STATES

F. S. Stephens

Lawrence Berkeley Laboratory
University of California
Berkeley, California 94720

I. Introduction

High-spin nuclear states are interesting at the present time, both because they are experimentally accessible, and because there have recently been several rather dramatic changes observed at high spins, and others even more dramatic are predicted. I want to begin by describing very briefly just what these are, what we now know about them, and what we are currently trying to find out about them. I will not go into any detail about the predicted properties of high-spin states because I am sure Prof. Szymanski will cover that subject in some depth in the next talk.

One of the changes occurring in high-spin states is the reduction and eventual quenching[1] of the pairing correlations. There is now strong evidence[2] that the pairing is, indeed, decreasing with increasing spin even at the lowest spin values. However, it is also reasonably clear that it has not disappeared by spin 20 ħ in many rare-earth nuclei. It is certainly an interesting experimental problem to determine just where and how the pairing is quenched, and I will show you some results later that suggest there may still be some pairing left at ~35 ħ in at least one case.

Changes in the nuclear shape are a second type of effect expected to occur with increasing spin. Small increases in deformation are known[3] to occur at low ($\lesssim$ 12 ħ) spin values in a number of nuclei with moderate or small deformation, and a rather sudden change from slightly oblate to rather strongly prolate shapes has been observed[4,5,6] in several light Hg nuclei. The liquid drop model (with rigid-body moments of inertia predicts[7] oblate shapes to be most stable up to high spin values (50 to 70 ħ for A $\approx$ 160) and then triaxial shapes with increasing deformation leading to fission (at 70-80 ħ). According to recent calculations[8,9] the shell corrections do not change the basic liquid-drop tendencies. The

prolate-deformed rare-earth nuclei, for example, are predicted to become (or tend to become) oblate via triaxial shapes at moderate spin values (30-50 $\hbar$) and then follow the liquid drop estimates. Two interesting conclusions from both the liquid-drop and the rotating-deformed-oscillator calculations are that there should be very high-spin isomeric states in the oblate region and also rapidly increasing moments of inertia in the triaxial region preceding fission. I will describe later how these effects are being searched for at the present time.

A third phenomenon that is expected to occur at high-spin values is the alignment of individual particle angular momenta. This is the dominant structure of the low-energy high-spin states in spherical and near-spherical nuclei, as is well known, and this process should compete with collective motion at higher spin values in the more deformed nuclei. Recently a model[10] involving the alignment of the angular momentum of an odd nucleon with that due to the core rotation has had considerable success for many weakly deformed nuclei. However, it is not yet entirely clear to what extent the core motion must be purely rotational in such a model. Also, it now seems rather likely that the "backbending" which has been observed[11] in some of the light rare-earth nuclei is due to the alignment[12] of two particular nucleons ($i_{13/2}$ neutrons in this mass region) with the core rotation. If the oblate shapes predicted by the liquid drop model are reached, all the angular momentum would be carried by aligned particles. This would be signaled rather unambiguously by the occurrence of the high-spin isomeric states mentioned above. Thus, at least three effects--loss of pairing, shape changes, and alignment--are known to be occurring in nuclei as the spins increase, and the interplay and competition of these (and perhaps still other) processes makes the study of high-spin states rather exciting at the present time.

II. Production of High-Spin States

There are two fairly common methods of producing high-spin states in medium and heavy nuclei. These are Coulomb excitation and heavy-ion compound-nucleus reactions. The highest spin values that might be reached by Coulomb excitation are only around 30 ħ in the most favorable cases (Pb projectiles and heavy, strongly deformed nuclei as targets); however, this method of production is very clean and offers the possibility of measuring a number of other properties of the high-spin states (lifetimes, magnetic moments, etc.). As an example[13] of what can be done in this direction at the present time, the spectra from thick ^{174}Yb and ^{176}Yb targets Coulomb excited by 585 MeV ^{136}Xe projectiles are shown in Fig. 1. The strongly Doppler-broadened lineshapes for the higher spin states are apparent, and these are both an advantage and a disadvantage for this method. They make the observation of still higher spin states much more difficult, but they contain information about the lifetimes of the states. The fits to these lineshapes from the ^{174}Yb target are shown in Fig. 2, together with the resulting mean lifetimes (accurate to 10-15%). To sharpen up these lines, one must restrict the projectile scattering angle, and an attempt to do this is shown in Fig. 3. Here gamma-ray coincidences were taken with ^{136}Xe ions scattered through angles between 80 and 100°, and although the resulting lines are still 10-12 keV wide, states as high as 20 ħ can be seen. Using longer runs, it should be possible to identify an additional one or two states with ^{136}Xe projectiles, and an additional three or four states using ^{208}Pb projectiles. Nevertheless, the Coulomb excitation method generally cannot compete with the heavy-ion compound-nucleus method in regard to producing the highest spins. A notable exception is in the trans-lead region where fission severely limits the compound-nucleus method (see contribution, pg. 77).

The highest spin states currently known to be populated in nuclei, 65-70 ħ, are produced in the evaporation residues following heavy-ion compound-nucleus reactions and the rest of this talk will be devoted to this method. The data divide rather naturally into two parts: those based on discrete gamma-ray lines observed in the evaporation residues ($I \lesssim 20$ ħ); and those based on the unresolved lines, or the so-called continuum ($I \gtrsim 20$ ħ). I will discuss later the reason for these two types of spectra. The discrete lines have been a subject of study for over ten years, and a considerable body of data has been accumulated. Since all except one (p. 64) of the experimental contributed papers on high-spin states deal with this type of data, I have decided to try to balance things somewhat and discuss mainly the continuum gamma rays. These contain the information about the highest spin states we presently know how to populate in nuclei.

III. Continuum Gamma Rays

1. Introduction.

An important aspect of the de-excitation of an evaporation residue from a heavy-ion compound-nucleus reaction is the distribution of angular momentum into the various reaction channels. The relevant features of this distribution can be demonstrated using the simple sharp-cutoff model.[14] Fig. 4 is a plot of energy versus angular momentum squared in the nucleus ^{166}Yb. The lowest energy states having a particular angular momentum value are called the yrast states, and the sloping line in Fig. 4 gives an estimate of the location of these states. The initial excitation energy and angular momentum range deposited in ^{166}Yb from the reaction ^{84}Kr + ^{82}Se → ^{166}Yb* at 327 MeV is given by the horizontal line. A nice feature of this plot is that there is equal population along this line. The energy available for neutron evaporation is roughly the difference between the excitation energy and the yrast energy, and thus it varies from nearly zero at high ℓ to the full excitation energy (60 MeV) at very low ℓ. Since a neutron binding plus kinetic energy is about 10 MeV in these nuclei, one fewer neutron will be emitted for each additional 10 MeV of yrast energy. This divides the population into "bins" as is illustrated in Fig. 4, where every full bin has equal population. In fact, above some particular angular momentum (about 50 $\hbar$ for ^{166}Yb) fission dominates over neutron evaporation and the bins are irrelevant (dashed in Fig. 4). The important point of this is that channels corresponding to different numbers of evaporated neutrons should have different angular momentum ranges, and the highest angular momenta are in the channels with the fewest evaporated neutrons. This fractionation is a very great help in studying angular-momentum effects in these nuclei.

Numerical studies of the de-excitation of an evaporation product from a heavy-ion compound nucleus were made by Grover[15] some time ago, and seem to be remarkably well borne out by subsequent experiments. Grover's proposed gamma-ray de-excitation of the product nucleus (with some later additions[16]) is illustrated in Fig. 5, which is a plot of energy versus spin in a rotational nucleus with mass around 160. The heavy bar in Fig. 5 is an estimate of the energy and angular momentum range left in this final product nucleus following an (^{40}Ar,4n) reaction. This energy is roughly a neutron binding energy above the yrast line, and the angular momentum range is limited by the 3n and 5n reactions as was discussed above. The gamma-ray de-excitation of the populated region is expected to occur in three distinct cascades. While the level density is high,

a statistical cascade (I) consisting mainly of high-energy dipole transitions is expected to occur. This carries off a considerable amount of excitation energy, but very little angular momentum, and is terminated by coming into the yrast region where the level density is no longer high. Grover has estimated that the gamma-ray spectrum from this cascade should fall off approximately exponentially in intensity with increasing energy above 2 MeV. In the yrast region the cascade is forced to begin carrying off angular momentum and proceeds by stretched E2 transitions through a number of collective bands roughly parallel to the yrast line. This is the yrast cascade (II) and it should produce a low-energy "bump" in the gamma-ray spectrum whose energy and shape contain information about the moments-of-inertia in the yrast region. Around spin 20 $\hbar$ the yrast levels become those of the ground-state band and an energy gap develops between these levels and others of the same spin. At this point all the population begins to shift into this particular band, producing individual transitions with sufficient intensity to be identified in the spectrum, that is, the discrete lines (III). Thus in the gamma-ray spectrum there should be three discernible features: very low energy ($\tilde{<}$ 1 MeV) discrete lines; an unresolved relatively low-energy ($\tilde{<}$ 2.5 MeV) bump; and an unresolved high-energy exponential tail.

2. Experimental

Early studies[17,18] of the continuum gamma rays were made about 15 years ago, but two developments were necessary before much progress in this area could be made. The first was a means to separate out specific reaction channels, and Sunyar and coworkers[19,20] first did this in 1972 using a Ge(Li) coincidence detector and selecting as gates the particular discrete lines that belonged to a known product (reaction channel). The second development was a technique to discriminate against neutron pulses, and several groups[21,22,23] have accomplished this recently by time-of-flight techniques. The experimental arrangement currently used in Berkeley is shown in Fig. 6. The beam strikes a thin (~1 mg/cm^2) target on a thick (~25 mg/cm^2) lead backing. An intrinsic Ge detector, located at 225° relative to the beam direction and 5 cm from the target, is used to select particular gamma ray lines corresponding to individual reaction channels. The continuum spectrum is observed in coincidence with the Ge detector in each of three 7.5 × 7.5 cm NaI detectors at 0, 45, and 90° relative to the beam direction and 60 cm from the target. The neutrons require 20 nsec to reach the NaI detectors and can be almost completely separated from the gamma rays, which require only ~2 nsec. The large distance also makes corrections for the pile-up

of pulses in the NaI detectors very small. With this arrangement it takes about a day to accumulate reasonable continuum spectra from an average reaction channel.

In order to clarify the method of channel selection, a spectrum taken[24] in the Ge detector from the reaction $^{84}Kr + ^{82}Se \rightarrow ^{166}Yb^*$ at 345 MeV, is shown in Fig. 7. The lines from Coulomb excitation of ^{84}Kr and ^{82}Se are unusually prominent in this spectrum due to the very heavy projectile, but previously known lines from the 3n, 4n, and 5n reaction channels can be easily identified. In the analysis of the data (stored event by event on magnetic tapes) we set gates on all the lines of interest, subtract backgrounds as determined from energy regions adjacent to these lines, and then sum up the spectra for all lines from a given reaction channel. We have not yet found statistically significant differences between the continuum spectra in coincidence with different lines from the same reaction channel. Thus three channels from this reaction can be studied simultaneously. Other groups have used different methods for selecting reaction channels of interest: Newton et al.[21] have used neutrons as trigger pulses and thus observed the composite continuum spectrum of all neutron-evaporation channels; and Albrecht et al.[23] have used particle detectors to select quasi-fission events. Many such possibilities exist.

3. Multiplicities

An important quantity to measure is the average number of gamma rays in the continuum spectrum, which has been called the multiplicity of the spectrum ($\bar{N}_\gamma$). This is easy to obtain provided one stores the singles events from the Ge counter, as well as the coincidences. Under the assumptions (a) that the probability of detecting two gamma rays simultaneously in the NaI detector is negligible, and (b) that the gating gamma ray, γ_i, is not in the continuum region being studied, the multiplicity associated with γ_i is just:

$$\bar{N}_\gamma(\gamma_i) = \frac{I_{coinc}(\gamma_i)}{I_{sing}(\gamma_i)\ \varepsilon_{NaI}} \qquad (1)$$

where $I(\gamma_i)$ is the total number of counts in the (singles or coincidence) peak of γ_i and ε_{NaI} is the roughly energy-independent probability of detecting a gamma ray in the NaI detector (including both the geometry and efficiency of the NaI detector). A problem exists at the low-energy region of the continuum spectrum, since the discrete lines in most deformed rare-earth nuclei extend

up to about 0.6 MeV and must then be subtracted. Also, the NaI efficiency is not so constant below this energy. Since rather few continuum gamma rays are expected below 0.6 MeV, our policy has been to work only with multiplicities for gamma rays with energies greater than this value; but some of the other groups have studied the continuum spectrum at lower energies.

The general result from all groups[20-26] that have studied multiplicities in evaporation residues following heavy-ion reactions is that they depend mainly on the angular momentum input to the channel, and are always sufficiently large so that the gamma rays can carry off that angular momentum. Thus the multiplicities vary rather strongly in different channels from the same reaction, as suggested by Fig. 4, and they also vary with bombarding energy for a given reaction channel. This result is illustrated in Fig. 8, where the multiplicities of various decay channels of the compound nucleus, $^{166}Yb^{*}$, are plotted against the average angular momentum in the channels. These average angular momenta ℓ_{av} were determined from the sharp-cutoff model and measured channel cross sections. It is apparent that the multiplicity does not depend strongly on the method of formation of the $^{166}Yb^{*}$, or on the particular product nucleus, but only on the angular momentum input. Furthermore, the number of gamma rays is reasonable. For the cases where ℓ_{av} is greater than ~25 $\hbar$, most of the transitions are of stretched E2 character and thus remove 2 $\hbar$ from the system. At ℓ_{av} = 30, the multiplicity is 10, corresponding to 20 $\hbar$ carried off by continuum gamma rays. In this case there are on the average, 5 known discrete lines at the bottom of the cascade which carry off the last 10 $\hbar$. Thus the 30 $\hbar$ indicated by the cross section is accounted for. In cases where the cross sections are not measured, ℓ_{av} can be estimated in this way from the multiplicity, provided the angular distributions show that the transitions are mostly of stretched E2 character.

The multiplicities can be used to study reaction mechanisms. Albrecht et al.[23] have used multiplicities to estimate the angular momentum deposited in the fragments, and hence the orbital angular momentum transferred (12-15 $\hbar$), in deep-inelastic scattering (quasi fission) events for the system ^{16}O + Ni. Higher moments of the number distributions have been determined by Hagemann et al.[25] by measuring higher order multiple coincidences. These authors obtain not only the multiplicity (first moment) but also the average variation in the number of gamma rays (second moment) and even a hint of the "skewness" of this spread (third moment). It is clear the the multiplicities will have many applications to studying reaction mechanisms, but that direction will not be pursued further here.

4. Energies

Probably the most interesting aspect of the continuum gamma-ray spectrum is its energy distribution, since this is the source of any information about moments-of-inertia at very high spin values. The observed pulse-height spectrum must first be corrected for the response function of the NaI detector. This is straightforward, though our procedure makes the statistical variations of the spectrum much worse. I will refer to the corrected gamma-ray spectrum as "unfolded" and the original pulse-height spectrum as "raw." Further small corrections for the motion of the emitting nucleus must be made to these unfolded spectra. An important related quantity is the energy-dependent angular distribution of the spectrum, and this is obtained simply by comparing the corrected 0, 45, and 90° spectra. The interpretation of these distributions is a bit complicated, since a beam-γ-γ triple correlation is involved. However, with the Ge detector at 225° this correlation for the NaI detectors resembles the usual beam-γ correlation, that is, a 0°/90° ratio of ~1.4 for stretched quadrupole transitions and ~0.7 for stretched dipoles. Thus it is possible in a simple way to determine something about the character of the transitions at each energy.

In Fig. 9 are shown the raw and unfolded gamma-ray spectra,[22] together with their 0°/90° intensity ratios, for 183 MeV ^{40}Ar projectiles on three targets, natural Cu, ^{82}Se and ^{126}Te. These are "gross" spectra, that is, spectra in coincidence with all gamma-ray pulses in the Ge detector, rather than separated channel spectra, but the general features are the same and the statistics are much better in this case. Above 2.5 MeV the exponential tail is quite clear in all three cases, both in the raw and unfolded spectra. The slopes are all similar, and correspond roughly to Grover's calculated slopes. The corrected angular distributions (dashed lines) indicate that this portion of the spectrum is not composed entirely of stretched quadruple transitions. All these features agree with the expectations for the statistical cascade, and it seems very likely that this is the origin of this part of the spectrum. Below ~2.5 MeV, a rise above the exponential tail is seen in all three cases, though the detailed characteristics of this bump differ considerably from case to case. In each nucleus the bump is accompanied by a rise in the 0°/90° intensity ratio, very likely indicating a higher proportion of stretched E2 transitions. Furthermore, the bump intensity and maximum energy increase with increasing angular momentum in the channel. These properties strongly suggest that this feature corresponds to the yrast cascade. Thus even without separating the individual reaction channels,

the general features expected for the continuum spectrum are rather clearly observed. We will now go on and extract more detailed information from some of these spectra.

There are two methods that one might use to extract moments of inertia from these continuum spectra, and both will be explored. The first involves the identification of a transition energy and its association with a spin value.[22] It turns out to be possible to do this for the maximum spin of each channel in the following way. Fig. 10 shows the raw and unfolded spectra for the 4n channel (^{162}Yb) from the bombardment of ^{126}Te with 183 MeV ^{40}Ar ions. The difference between the 0° and 90° spectra is also shown. The important point is that there is a rather sharp upper energy edge to the bump transitions. This is seen especially clearly in the 0°-90° spectrum, where the stretched E2 transitions are enhanced over other types, but it is also quite apparent in the other spectra. This energy edge also shows up clearly for the other separated channels we have studied, and always varies in such a way that it is higher when higher angular momentum is introduced into the channel. This suggests that this highest energy in the channel is associated with the highest angular momentum in the channel, as would be expected for any normal behavior of moment of inertia with spin. A value for the maximum angular momentum in the channel can be obtained from the measured channel cross sections and the sharp-cutoff model, or can be estimated from the gamma-ray multiplicity as discussed in the previous section. As a result we can relate a maximum yrast transition energy, E_t, in a channel with a maximum angular momentum, I, and obtain moment-of-inertia values, $\mathcal{J}(I)$, according to the simple relation:

$$\frac{2\,\mathcal{J}(I)}{\hbar^2} = \frac{4I-2}{E_t} \qquad (2)$$

These values for several reactions leading to ^{166}Yb compound nuclei will be discussed below, together with those from the second method.

The height of the bump at a particular energy, E_t, corrected for the extension of the statistical tail, gives the number of collective transitions per energy interval. The reciprocal of this quantity, the energy interval between collective transitions, ΔE_t, can be related directly to a moment of inertia:[27]

$$\Delta E_t = 8 \frac{\hbar^2}{2 \mathcal{J}(E_t)} - 2E_t \frac{d \ln \mathcal{J}(E_t)}{dI} \qquad (3)$$

Since I can be obtained from eq. (2) for a given E_t and $\mathcal{J}(E_t)$, one can in general solve eq. (3) by iteration for a series of ΔE_t values. However, for the Yb nuclei in the spin range of interest, it is a reasonably good approximation to assume a constant moment of inertia, and thus neglect the last term of eq. (3). The moment of inertia is then obtained directly; however, two problems must be considered. First, the background due to the low energy part of the exponential tail is poorly known. It is not even clear whether it continues up with decreasing energy, or falls off, as one might expect theoretically. We have taken it to be constant and equal to its value just above the bump, but a 10 to 20% uncertainty is so introduced. The other problem is that this method only works provided the entire population goes through the spin region of interest, i.e. no side feeding. We can estimate that this might be a reasonable assumption for spins in a given channel below the maximum spin estimated for the lower adjacent channel. For the 4n reaction of 183 MeV ^{40}Ar + ^{126}Te, this limit would correspond to the I_{max} of the 5n channel, or about 35 $\hbar$. For all lower spin values this method should be approximately valid in the 4n channel. The enormous advantage of this method is that it can give moments of inertia continuously over a whole range of transition energies (spin values). Changes in the moment-of-inertia must show up as irregularities in the height of the bump at the appropriate transition energy. A study of Fig. 10 in the applicable energy interval -- 0.7 to 1.0 MeV -- shows that while some interesting irregularities could be occurring, the unfolded spectrum is flat within the statistical uncertainties, and thus we have evaluated just a single moment of inertia for this energy region.

The moment-of-inertia data for ^{162}Yb from the first method described above are shown as solid points on Figs. 11, which is a standard "backbending" plot, and the known low spin states of this nucleus have also been included. The open points are for adjacent nuclei, the odd-mass products of the 3n and 5n reactions at high spin values, and the isotone ^{160}Er (for which more states are known) at low spins. For comparison, the dashed line gives the rigid diffuse sphere value[28] for mass 162 with an effective sharp radius of 6.70 fermis. The horizontal line corresponds to the independent moment-of-inertia value obtained from the second method and covers the appropriate range of frequencies. The three shorter lines show the same data divided into smaller intervals (3

channels cf. Fig. 10), but our opinion is that this variation (and that of still finer intervals) might be just statistical. On Fig. 11 it is clear that the values obtained from the two methods are reasonable and in good agreement with each other. Also the high-spin odd-mass data do not differ significantly from the ^{162}Yb data. Since the deformed rigid-body value of the moment of inertia would be roughly another 10% larger than the value given for the rigid sphere, it does seem that the measured moment-of-inertia values might be a little lower than expected, at least up to I~35 $\hbar$. If so, this might indicate some residual pairing correlations at that spin value. It will obviously be of considerable interest to improve these methods in order to see more details of these moments of inertia.

These methods are equally applicable outside the deformed rare-earth region. The energy spectra[22] from the 4n and 6n channels of the reaction, ^{82}Se + ^{40}Ar, at 183 MeV, are shown in Fig. 12, together with the 4n channel from ^{126}Te + ^{40}Ar at the same energy. The effects are even more pronounced in these Te nuclei, and also correspond to higher spin values (due to reduced fission competition). Thus it appears that moments of inertia at high-angular momenta can be studied by these techniques over a broad region of the periodic table.

We are optimistic that these methods can give information about the changes (mentioned earlier) which might be occurring in these nuclei as the spin increases. The pairing strength can be estimated rather simply from the moment-of-inertia values, as mentioned above. The predicted rather rapid increase in deformation just prior to fission should be reflected in rapidly increasing moment-of-inertia values and this should be observed as a rise at the high energy end of the collective bump, in cases where sufficient angular momentum can be gotten into the channel. The Te nuclei discussed above are a good place to look or this effect. The isomeric states that should result from the high degree of particle alignment expected for oblate shapes should be easily observable between accelerator beam bursts provided some of them have lifetimes longer than ~ 1 nsec. Such experiments are extremely easy, though systematic searches have not yet been made. Thus it seems that this area of high-spin studies is currently open and rather exciting. It is hard to predict just what may come out of it in the next few years

IV. Conclusion

This paper has dealt mainly with the continuum gamma rays following heavy-ion reactions. Information is just beginning to come from such studies. The bulk of our information about high spin states in medium and heavy nuclei has come from studies of the discrete gamma-ray lines following these reactions. The beginning steps of all three effects I have discussed -- loss of pairing, shape changes, and particle alignment -- are seen in these studies for states having spins around 20 $\hbar$ or less. The contributed papers on high-spin states are concerned mainly with such studies, so that you will hear about some of the progress in this area. Coulomb excitation has thus far not contributed so much to our knowledge of high-spin states. But it is my opinion that when Xe and heavier beams become readily available, Coulomb excitation studies will show us some new aspects of high-spin states.

Acknowledgments

I am indebted to many people for discussions on these topics and thank especially Dr. R. M. Diamond for his comments and suggestions.

This work is supported under the auspices of the U. S. Energy Research and Development Administration.

REFERENCES

1. B. R. Mottelson and J. G. Valatin, Phys. Rev. Letters 5, 511 (1960).

2. R. A. Sorenson, Rev. Mod. Phys. 45, 353 (1973), and references therein.

3. R. M. Diamond, F. S. Stephens, K. Nakai, and R. Nordhdgen, Phys. Rev. C3, 344 (1971).

4. D. Proetel, R. M. Diamond, P. Kienle, J. R. Leigh, M. R. Maier, and F. S. Stephens, Phys. Rev. Letters, 31, 896 (1973).

5. N. Rud, D. Ward, H. R. Andrews, R. L. Graham, and J. S. Geiger, Phys. Rev. Letters 31, 1421 (1973.

6. D. Proetel, R. M. Diamond, and F. S. Stephens, Phys. Letters 48B, 102 (1974).

7. S. Cohen, F. Plasil, and W. J. Swiatecki, Annals of Physics 82, 557 (1974).

8. R. Bengtsson, S. E. Larsson, G. Leander, P. Möller, S. G. Nilsson, S. Aberg and Z. Szymanski, preprint, June, 1975.

9. A. Faessler, private communication, July, 1975.

10. F. S. Stephens, Rev. Mod. Phys. 47, 43 (1975), and references therein.

11. A. Johnson, H. Ryde, and J. Sztarkier, Phys. Letters 34B, 605 (1971).

12. F. S. Stephens and R. S. Simon, Nucl. Phys. A183, 257 (1972.

13. D. Ward, I. Y. Lee, P. Butler, R. S. Simon, P. Colombani, R. M. Diamond, and F. S. Stephens, unpublished data, 1975.

14. J. M. Blatt and V. F. Weisskopf, Theoretical Nuclear Physics (Wiley, New York, 1952).

15. J. R. Grover and J. Gilat, Phys. Rev. 157, 802 (1967); ibid 157, 814

(1967); ibid 157, 823 (1967; J. R. Grover, Phys. Rev. 157, 832 (1967).

16. J. O. Newton, F. S. Stephens, R. M. Diamond, W. H. Kelly, and D. Ward, Nucl. Phys. A141, 631 (1970).

17. J. F. Mollenauer, Phys. Rev. 127, 867 (1962).

18. Yu. Ts. Oganesyan, Yu. V. Lobanov, B. N. Markov, and G. N. Flerov, Soviet Phys. JETP 17, 791 (1963).

19. E. der Mateosian, S. Cochavi, O. C. Kistner, A. W. Sunyar, and P. Thieberger, Bull. Amer. Phys. Soc. 17, 530 (1972).

20. E. der Mateosian, O. C. Kistner, and A. W. Sunyar, Phys. Rev. Letters 33, 596 (1974).

21. J. O. Newton, J. C. Lisle, G. D. Dracoulis, J. R. Leigh, and D. C. Weisser, Phys. Rev. Letters 34, 99 (1975).

22. M. V. Banaschik, R. S. Simon, P. Colombani, D. P. Soroka, F. S. Stephens, and R. M. Diamond, Phys. Rev. Letters 34, 892 (1975).

23. R. Albrecht, W. Dünnweber, G. Graw, H. Ho, S. G. Steadman, and J. P. Wurm, Phys. Rev. Lett. 34, 1400 (1975).

24. P. O. Tjøm, F. S. Stephens, R. M. Diamond, J. de Boer, and W. E. Meyerhof, Phys. Rev. Letters 33, 593 (1974).

25. G. B. Hagemann, R. Broda, B. Herskind, M. Ishihara, S. Ogaza, and H. Ryde, Nucl. Phys. A245, 166 (1975).

26. M. Fenzl and O. W. B. Schult, Z. Physik 272, 207 (1975).

27. R. S. Simon, P. Colombani, M. Banaschik, D. Soroka, R. M. Diamond, and F. S. Stephens, to be published.

28. W. D. Meyers, Nucl. Phys. A204, 465 (1973).

Figure Captions

Fig. 1. Coulomb excitation of thick ^{174}Yb and ^{176}Yb targets with 585 MeV ^{136}Xe. The labeled lines are those of the ground-state rotational bands in these nuclei. The out-of-beam spectra were taken during the ~25 msec interval between the ~3 msec-long beam pulses of the SuperHILAC.

Fig. 2. Gamma-ray line shapes of four transitions in the ground-state rotational band of ^{174}Yb, Coulomb excited by 595 MeV ^{136}Xe. The errors on the measured mean lifetimes are 10-15%.

Fig. 3. Gamma-ray spectra from a thin target of ^{174}Yb taken in coincidence with ^{136}Xe ions scattered into angles between 80 and 100°. The upper spectrum has the additional requirement of a coincidence with a gamma ray of energy, $100 < E < 800$ keV, detected in either of two 7.5 × 7.5 cm NaI crystals.

Fig. 4. Plot of excitation energy vs. angular momentum squared for a nucleus with $A \approx 166$. The yrast line is drawn as that of a rigid rotor with $E = 0.009\ell^2$. The excitation energy and angular momentum range for the reaction ^{84}Kr + ^{82}Se → ^{166}Yb* at 327 MeV are also shown. The fractionation of the angular momentum into bins is indicated, as is the point where fission and other processes dominate over the xn products. The lines separating the bins are, of course, not completely sharp in a real case.

Fig. 5. Excitation energy is plotted against angular momentum for a nucleus (with mass around 160) that is the product of an (^{40}Ar,4n) reaction. The populated energy and angular momentum range is shown, together with the proposed gamma-ray cascades to the ground state.

Fig. 6. Sketch of the experimental arrangement used in Berkeley for studying continuum gamma rays.

Fig. 7. Singles Ge spectrum of 345 MeV ^{84}Kr on ^{82}Se, showing ground-band transitions in ^{162}Yb(4n), ^{161}Yb(5n), and ^{163}Yb(3n) together with

Coulomb-excited 2→0 transitions in ^{82}Se and ^{84}Kr.

Fig. 8. Average number of continuum γ-rays with $E_\gamma > 0.6$ MeV coincident with the lowest observed discrete transition ($2^+ \rightarrow 0^+$ or $17/2^+ \rightarrow 13/2^+$) vs. the average angular momentum in the reaction channel leading to that product. The circles, triangles and squares are for the 5n, 4n, and 3n reactions from $^{16}O + ^{150}Sm$ (open), $^{84}Kr + ^{82}Se$ (closed), $^{40}Ar + ^{126}Te$ (half-closed). The parentheses on the ^{84}Kr data indicate that considerable uncertainty in the values of $\bar{\ell}$ is introduced by the target thickness in this case.

Fig. 9. The raw (dots) and unfolded (triangles) continuum spectra in coincidence with the full Ge-detector spectrum for 183 MeV ^{40}Ar projectiles on Cu, ^{82}Se, and ^{126}Te targets. The straight lines are fitted to the unfolded spectrum between 3.2 and 6.2 MeV (solid portion) and extrapolated to lower energies (dashed portion). The upper plots show the 0°/90° intensity ratios for the raw data (dots) and for the unfolded data corrected for recoil motion (triangles). The error bars indicate statistical errors only.

Fig. 10. The raw (open circles) and unfolded (closed circles) continuum spectra from the $^{126}Te(^{40}Ar, 4n)^{162}Yb$ reaction channel at 183 MeV bombarding energy. Also shown (triangles) is the 0° minus 90° spectrum from this channel.

Fig. 11. Typical backbending plot (moment-of-inertia vs. square of rotational frequency) for ^{162}Yb and neighboring nuclei. The solid points are for ^{162}Yb (4n product) and the open points are for the 3n and 5n products measured by the first method described in the text. The lines correspond to the values determined by the second method described in the text, where the estimated uncertainty is shaded. Lower spin points for ^{162}Yb and the isotone ^{160}Er are also shown.

Fig. 12. The histograms show the raw continuum spectra in coincidence with the (background-corrected) γ-ray lines from the specific reaction products indicated. Negative or zero counts are plotted at the bottom of the figure. The dots show the unfolded spectra in the lower-energy regions where the statistical variations are not too large.

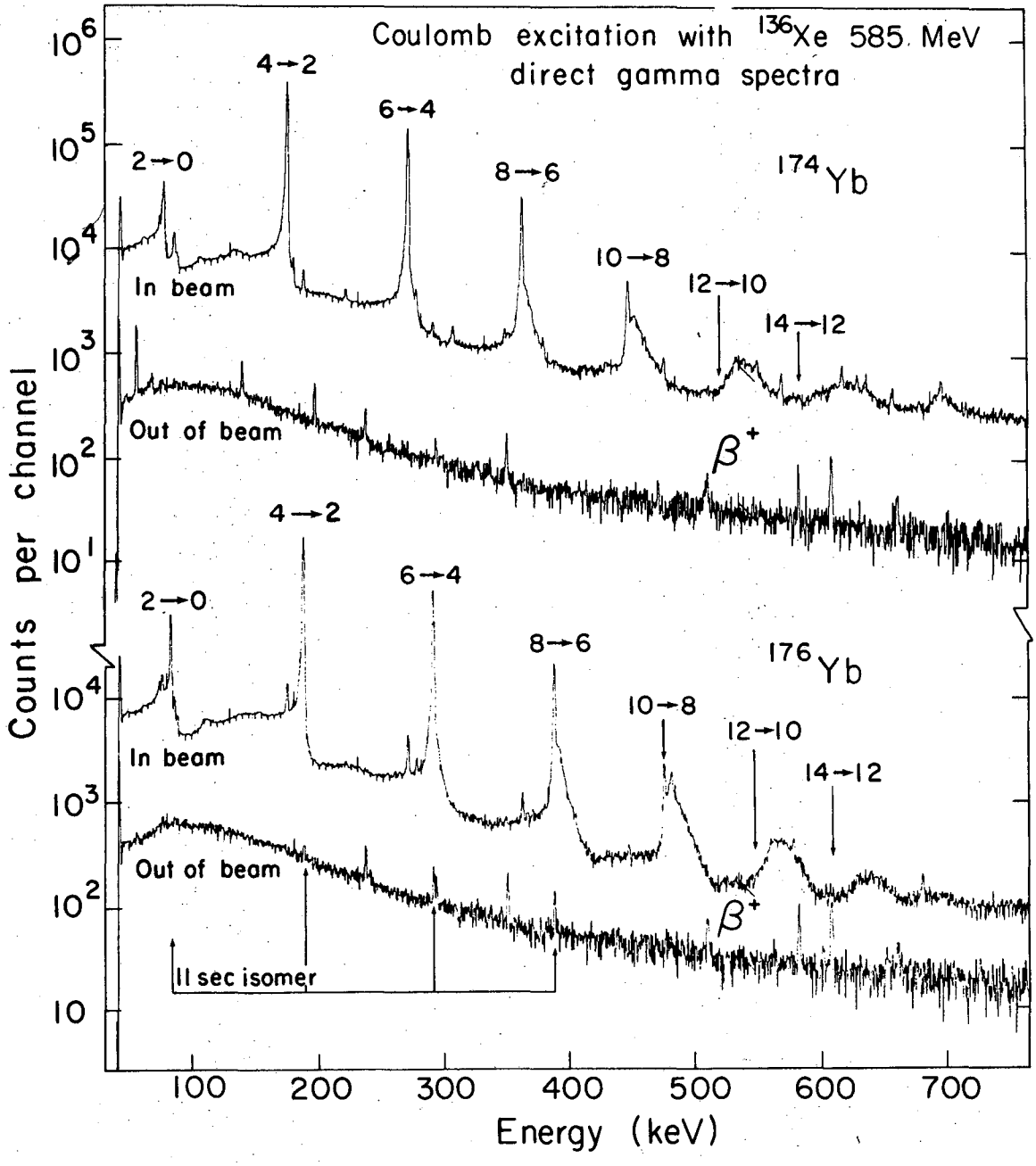

Fig. 1

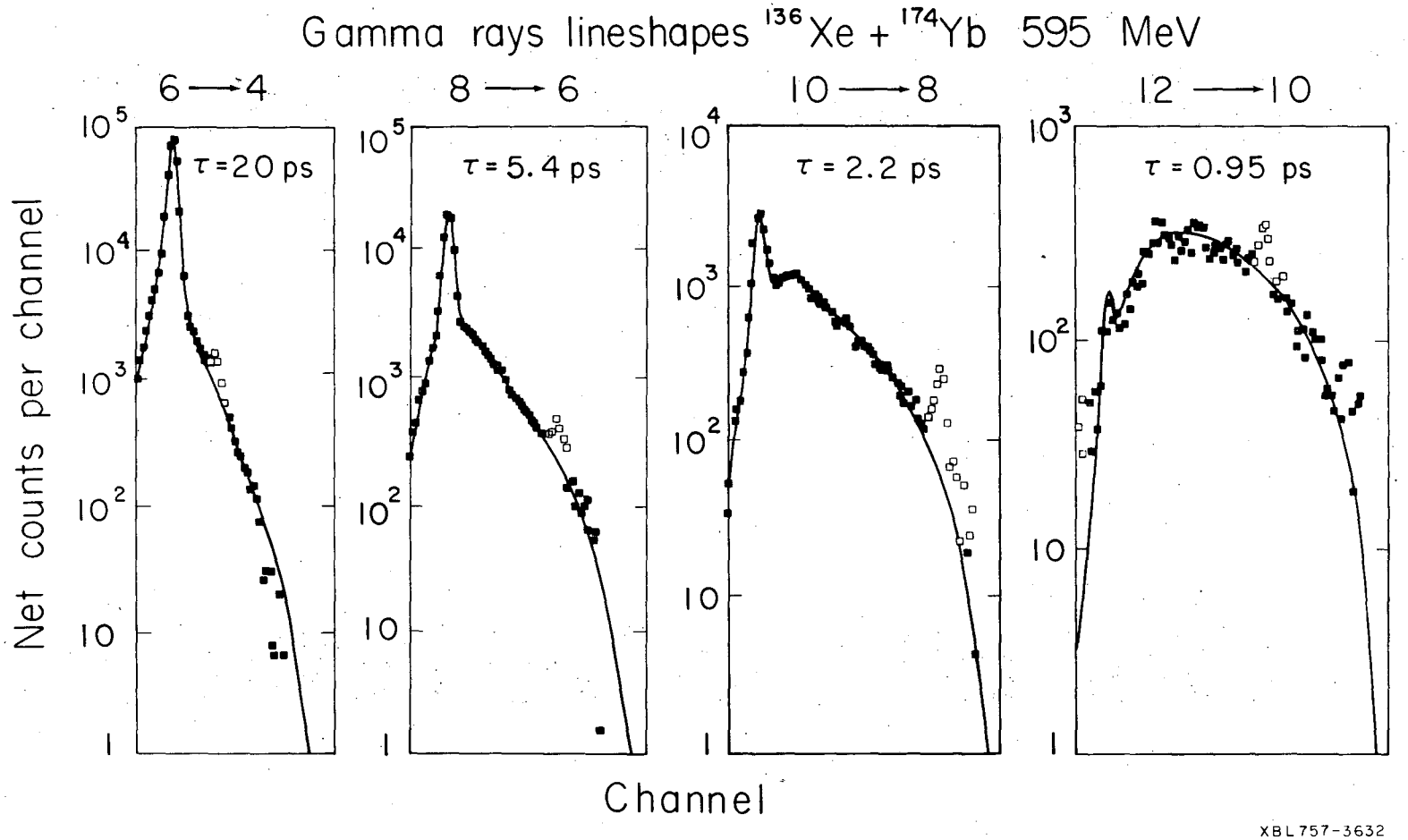
Gamma rays lineshapes ^{136}Xe + ^{174}Yb 595 MeV
6 → 4
8 → 6
10 → 8
12 → 10
τ = 20 ps
τ = 5.4 ps
τ = 2.2 ps
τ = 0.95 ps
Net counts per channel
Channel
XBL757-3632

Fig. 2

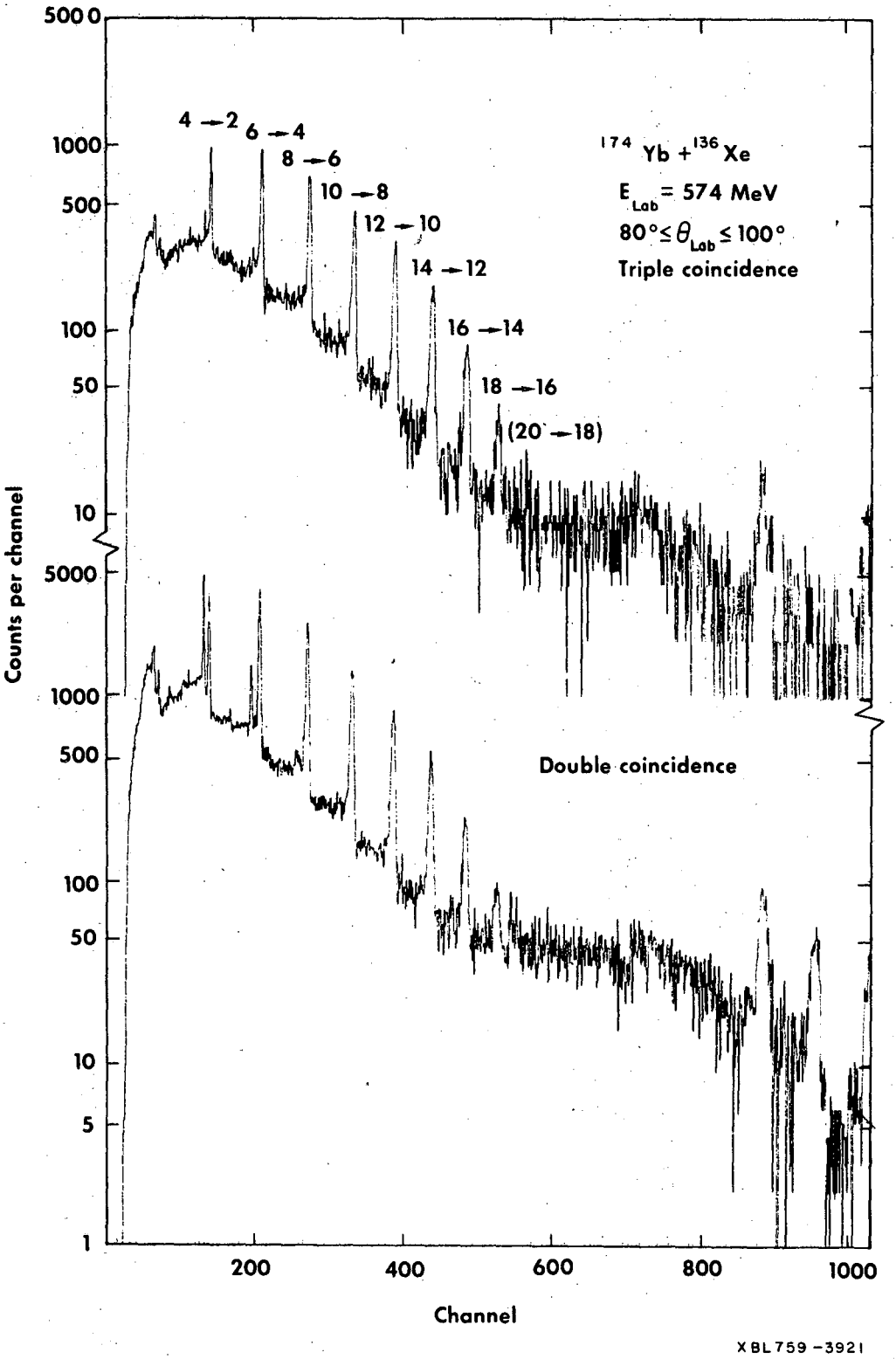

XBL759-3921

Fig. 3

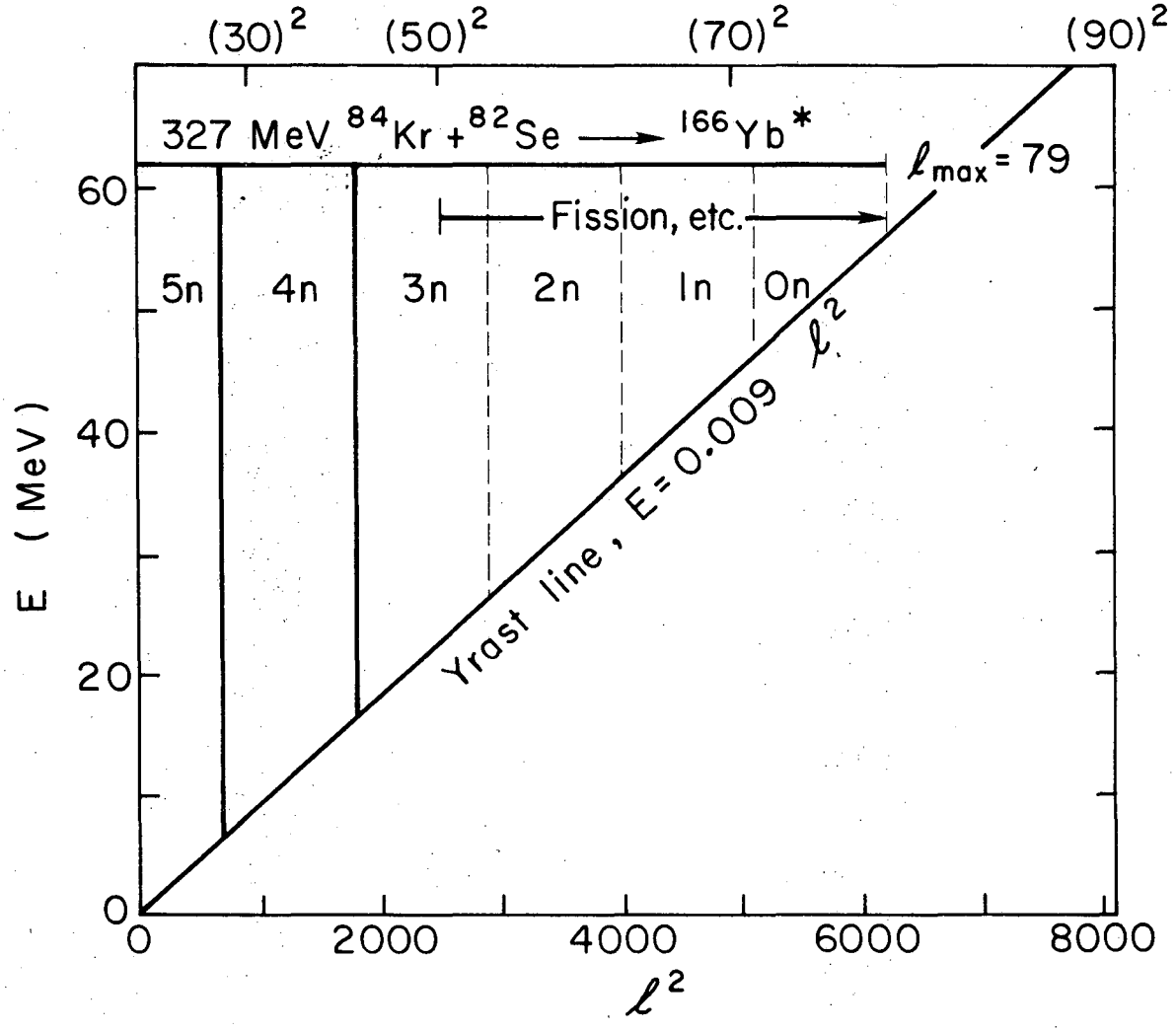

XBL759-3919

Fig. 4

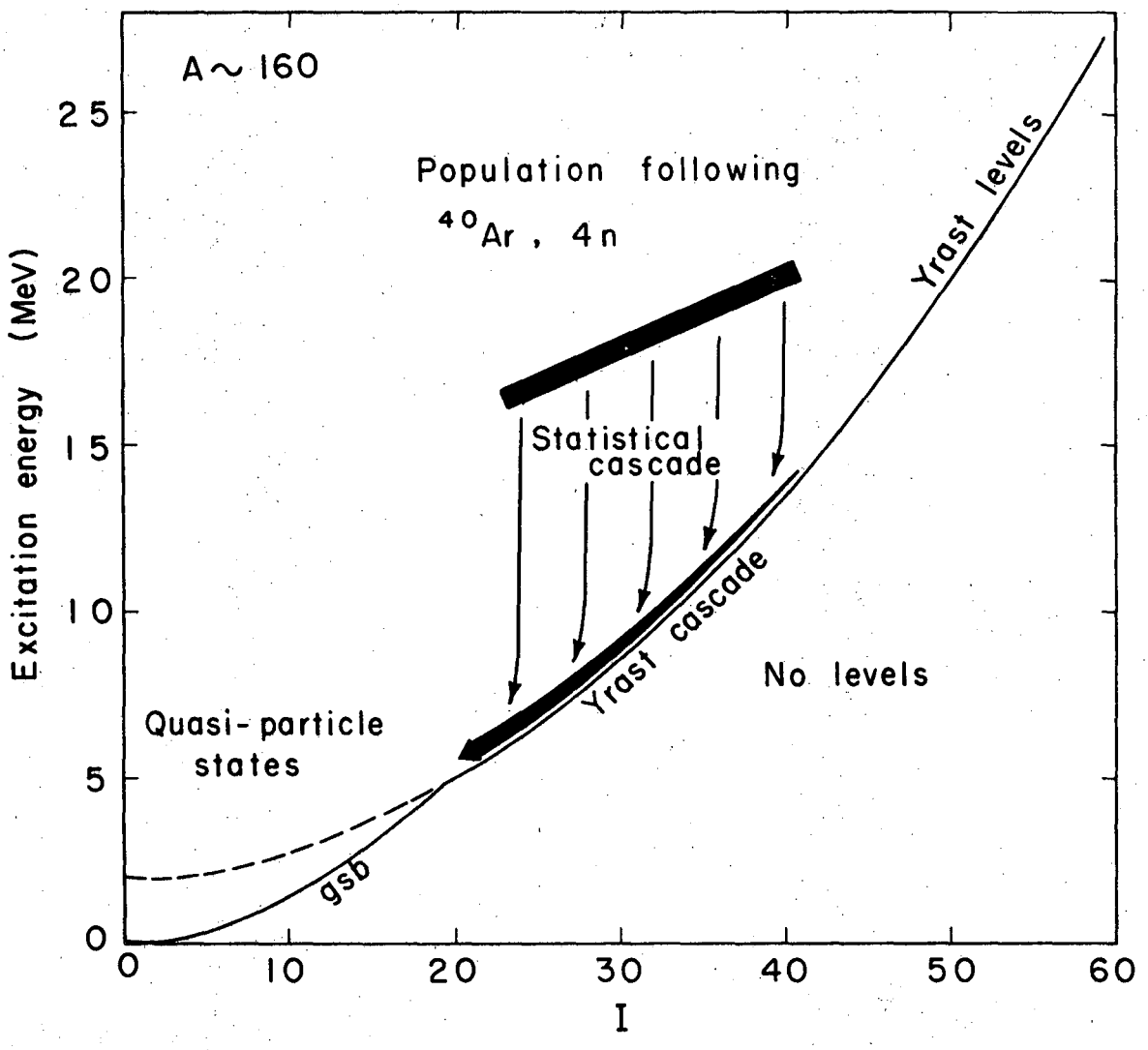

Fig. 5

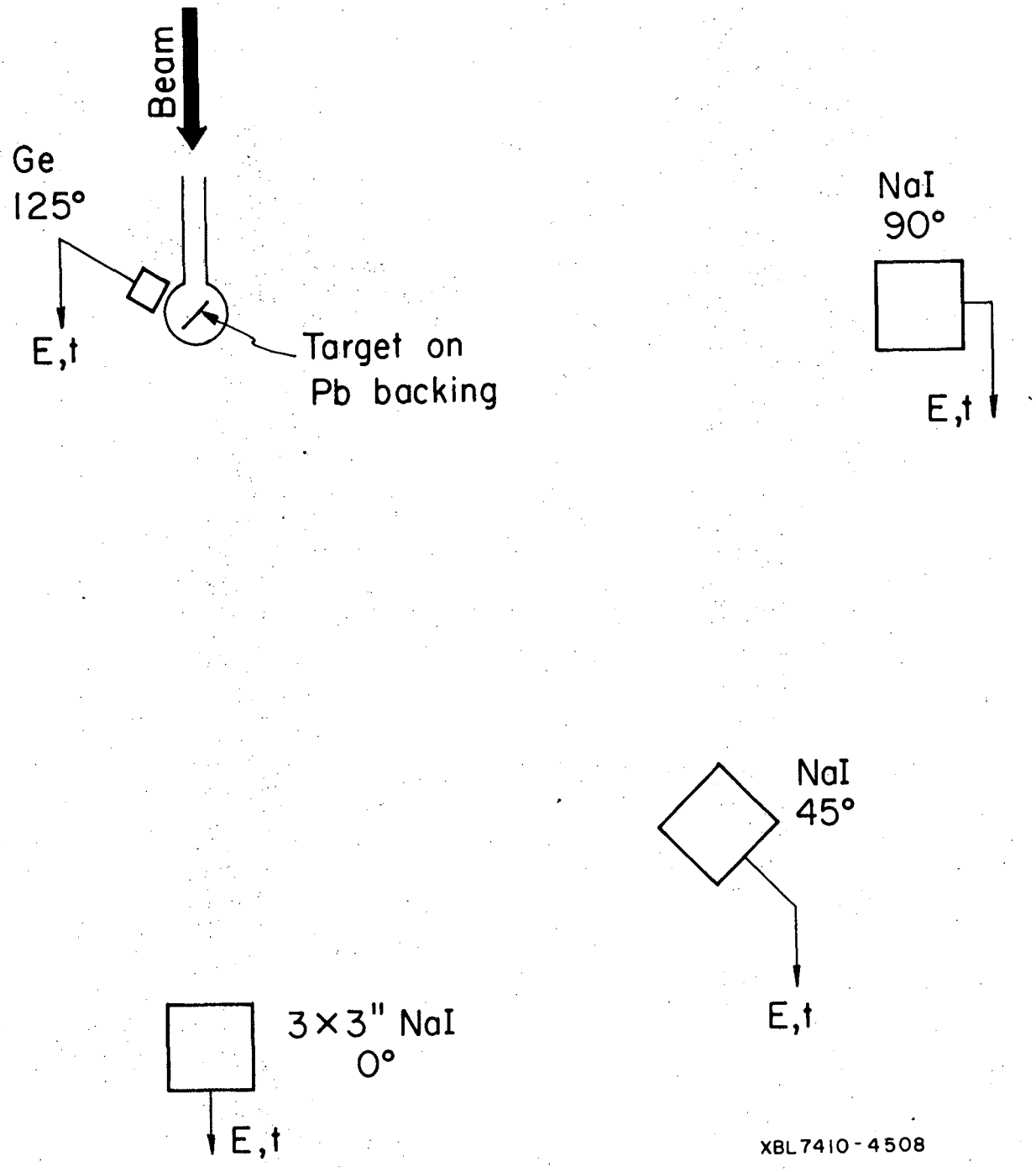
Beam
Ge
125°
E,t
Target on
Pb backing
NaI
90°
E,t
NaI
45°
E,t
3×3" NaI
0°
E,t
XBL7410-4508

Fig 6

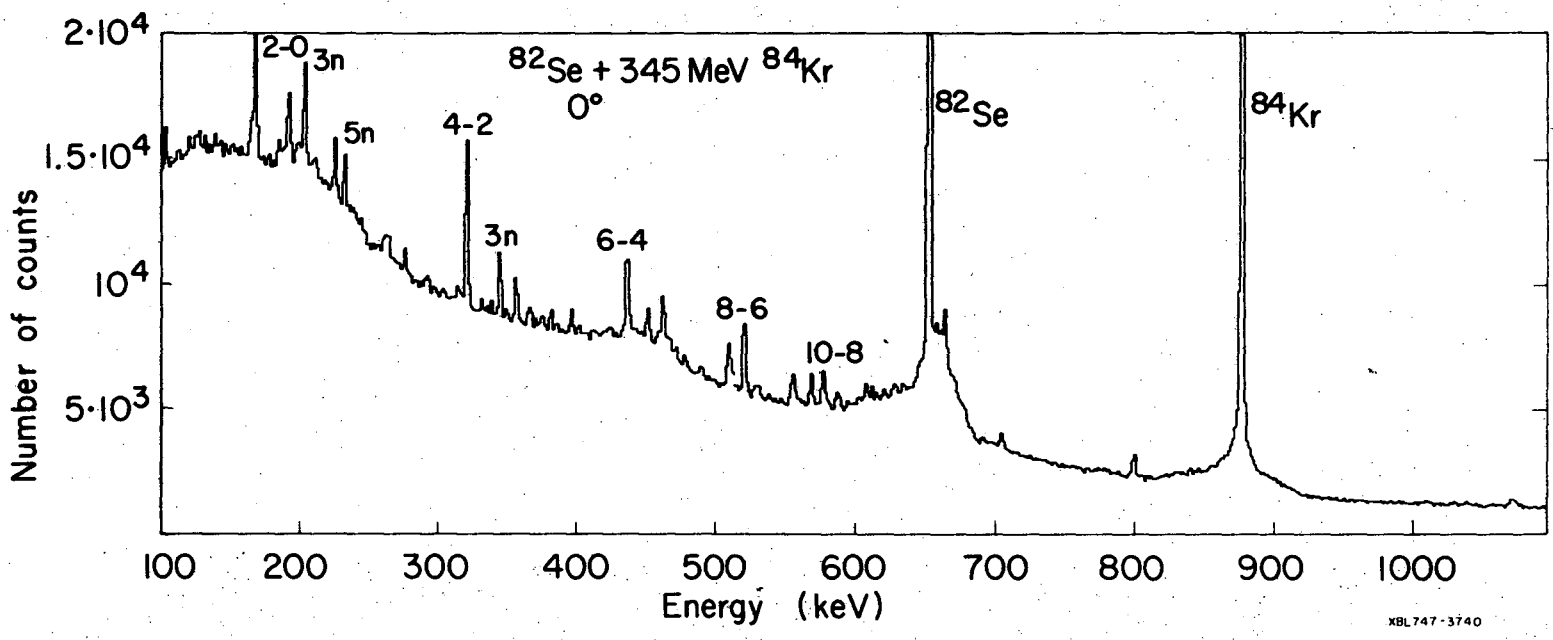

Fig. 7

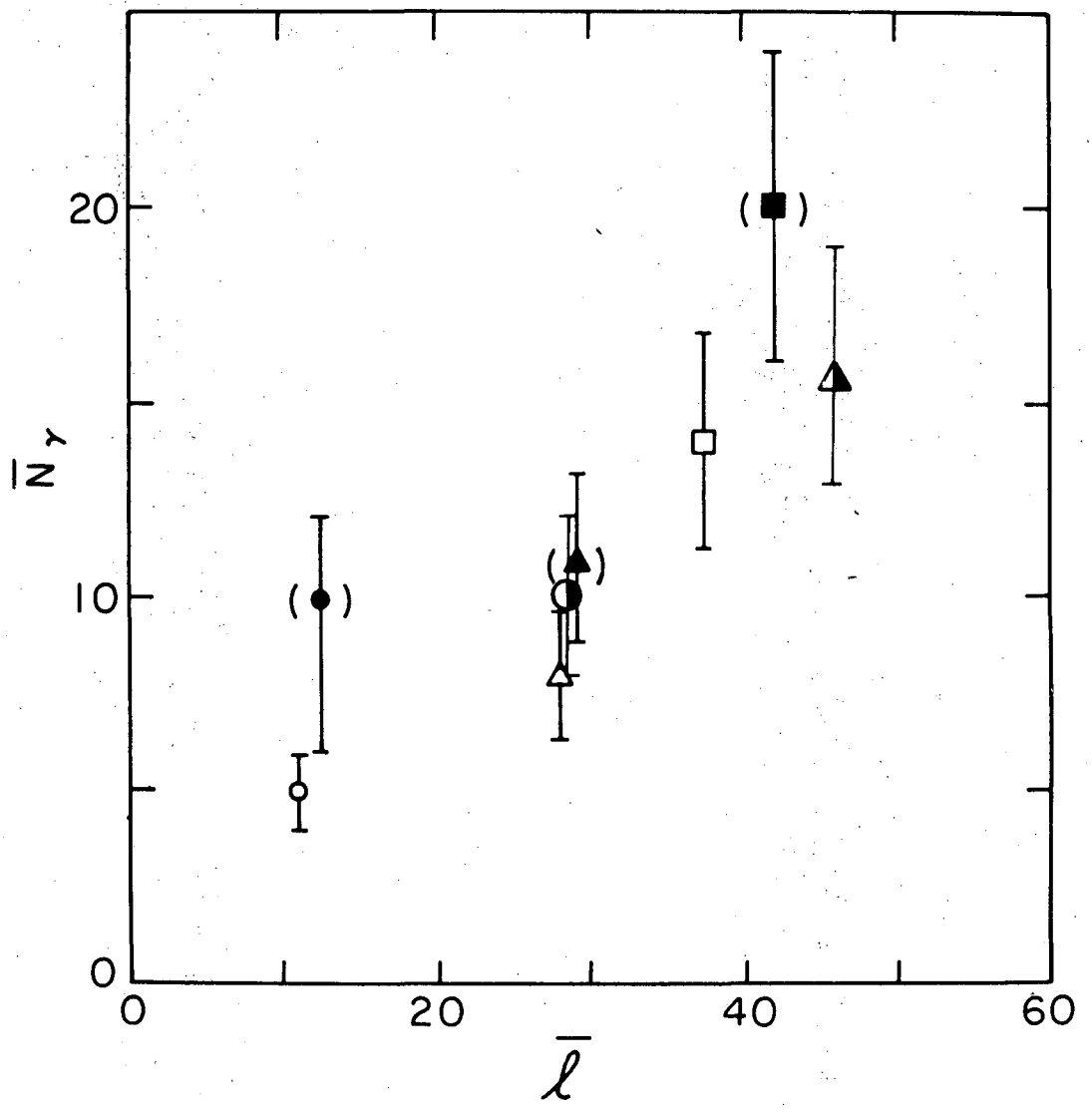

Fig. 8

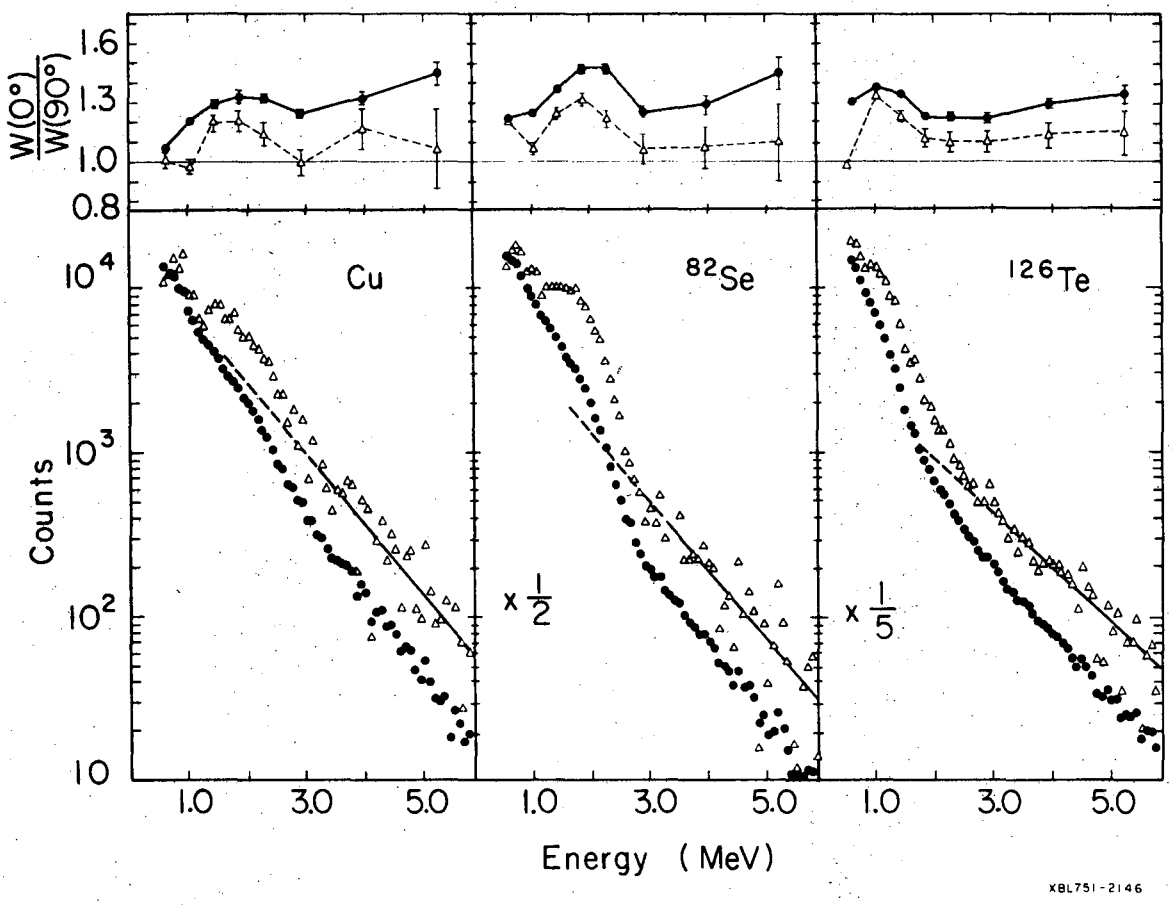

Fig. 9

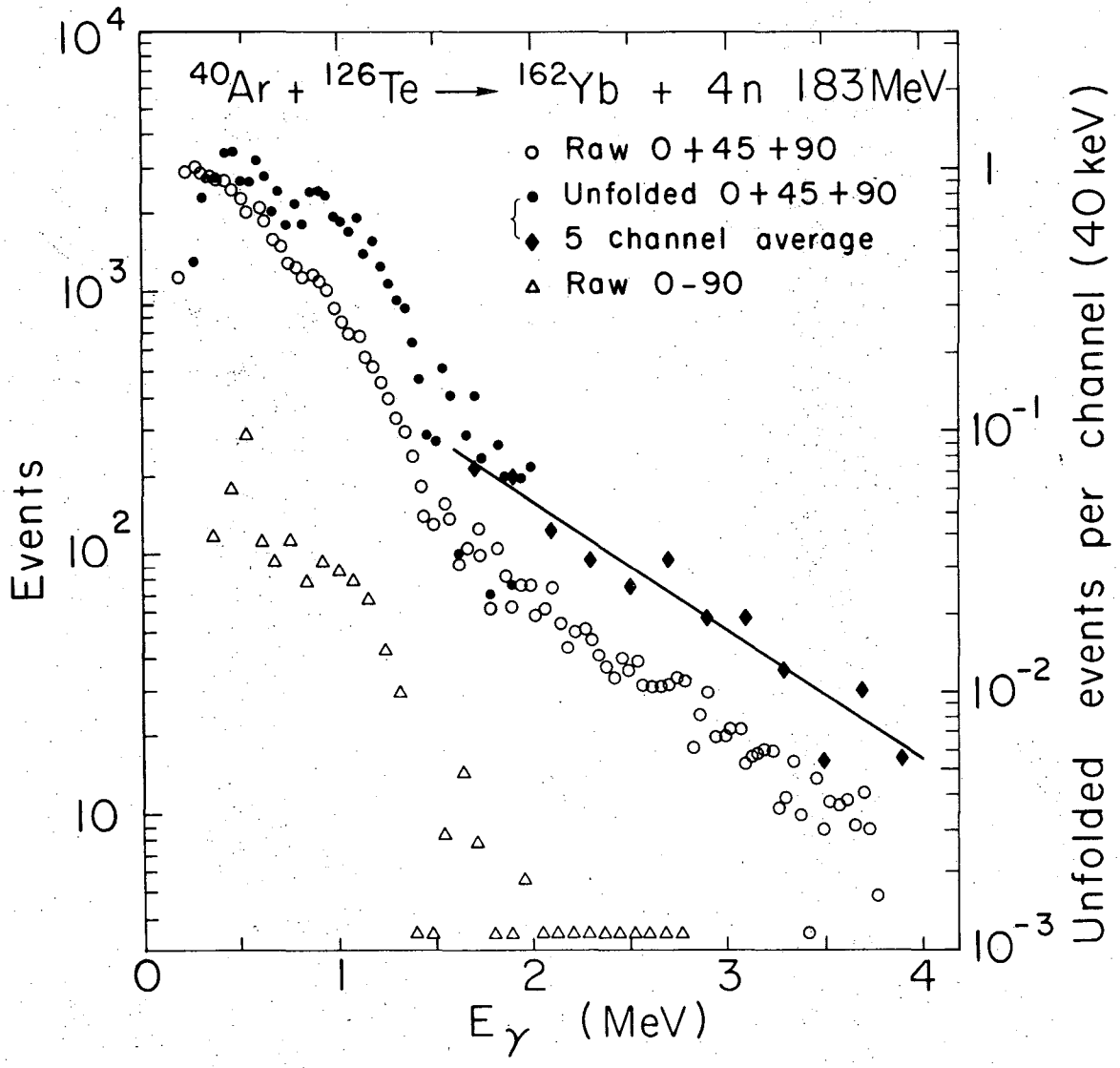

XBL759-3920

Fig. 10

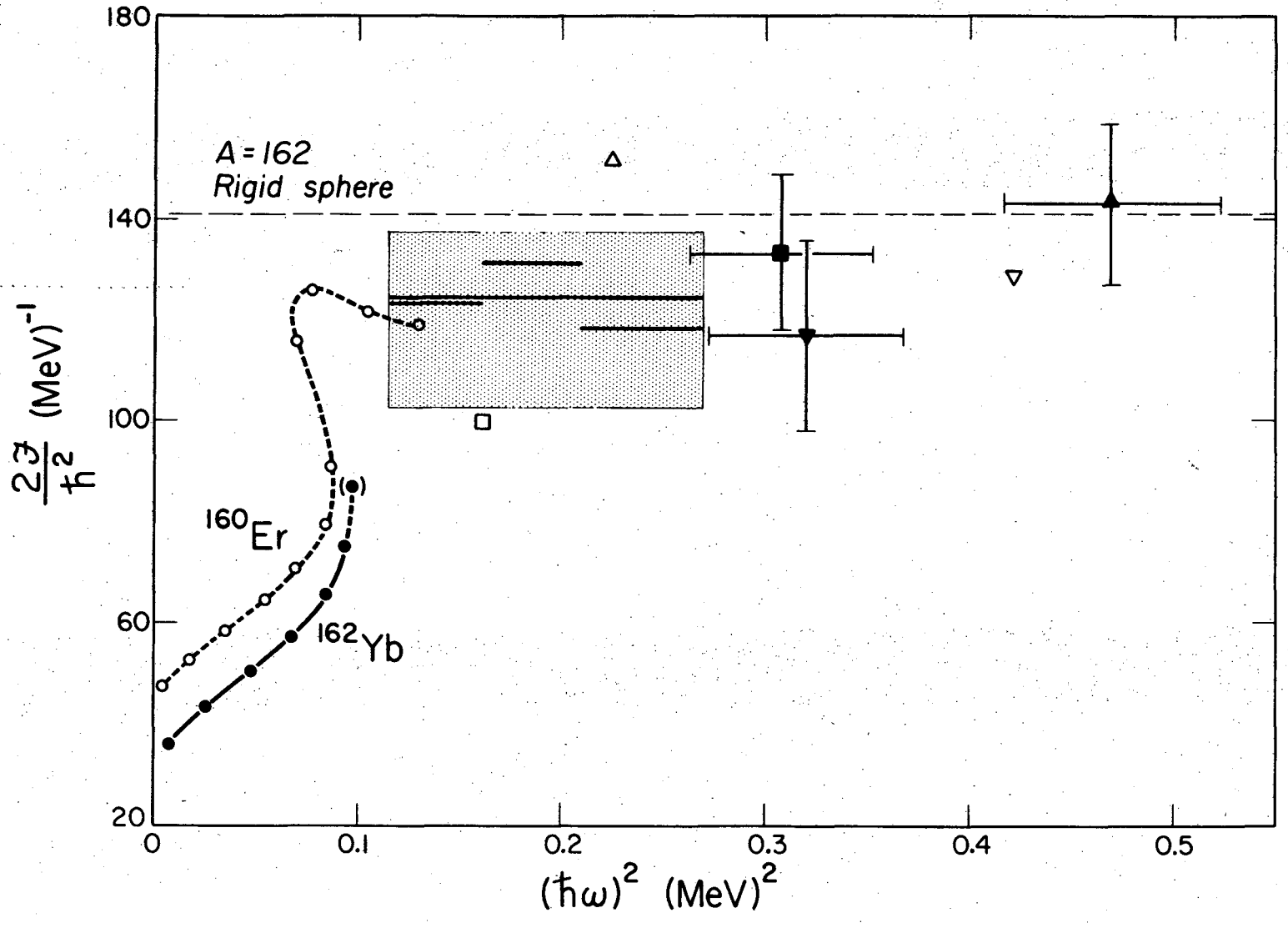

XBL 756-3235A

Fig. 11

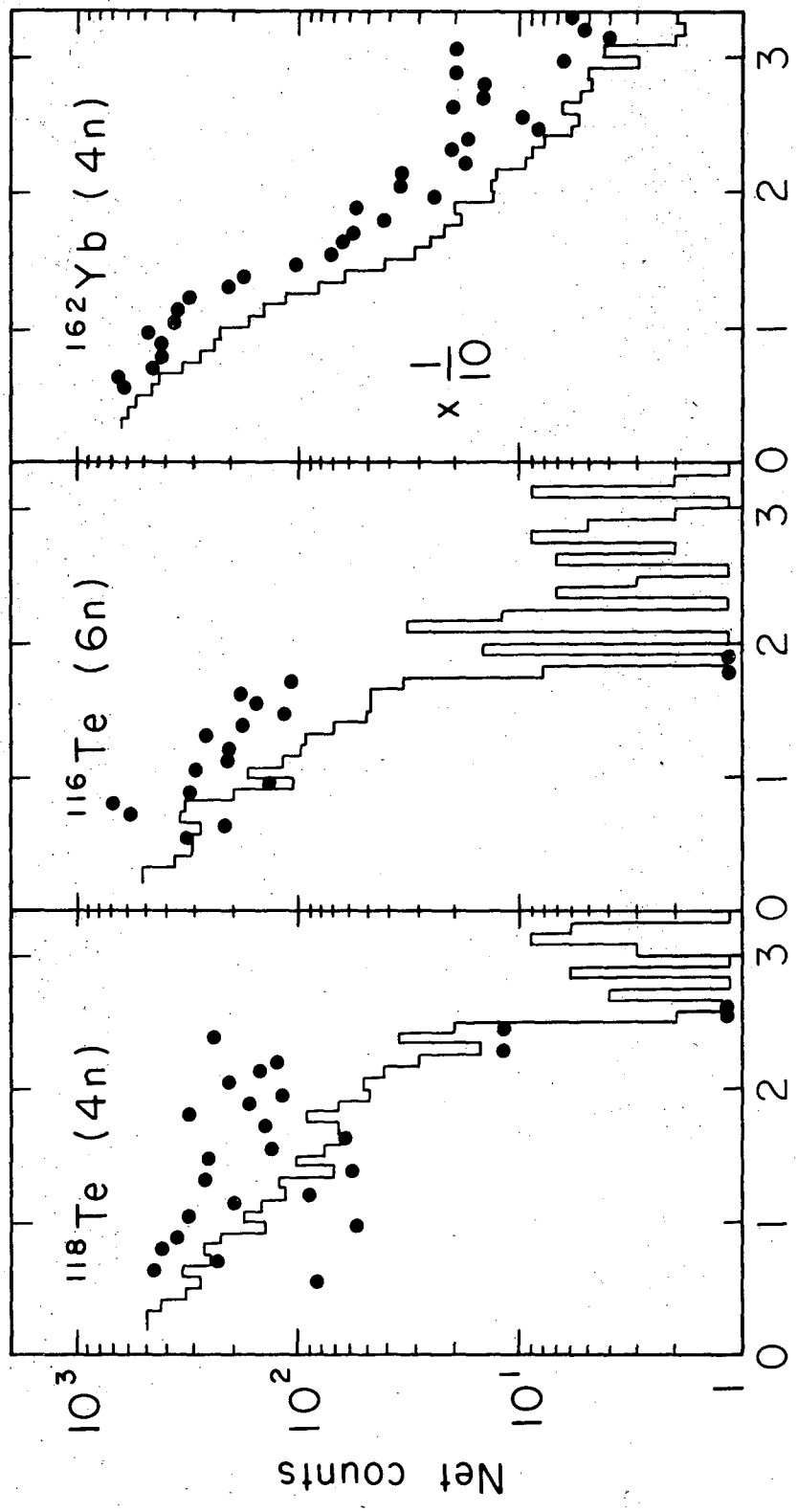
Net counts
10^3
10^2
10^1
1
^{118}Te (4n)
^{116}Te (6n)
^{162}Yb (4n)
$\times \frac{1}{10}$
0
1
2
3
Energy (MeV)
XBL752-2239

Fig. 12

TECHNICAL INFORMATION DIVISION
LAWRENCE BERKELEY LABORATORY
UNIVERSITY OF CALIFORNIA
BERKELEY, CALIFORNIA 94720